HIGH RESOLUTION X-RAY SPECTROSCOPY ON THE EINSTEIN OBSERVATORY

George W. Clark
Massachusetts Institute of Technology

My first trip to Huntsville was in 1959 when work began at the Redstone Arsenal on NASA's first astronomy satellite, Explorer XI, with a payload developed at MIT for detecting high energy gamma rays. It is a pleasure to return to Huntsville once again to join in the celebration of the success of NASA's most recent astronomy satellite, HEAO-2, and to tell about the early results from the Focal Plane Crystal Spectrometer (FPCS) developed at MIT for the Einstein Observatory.

Since the early days of X-ray astronomy it has been realized that detection and measurement of emission lines in X-ray spectra offer the prospect of new and detailed understanding about the physical conditions in X-ray sources. In the results from the Einstein Solid State Spectrometer, we have seen how emission features can be detected and identified by moderate resolution spectroscopy. However, many of these features undoubtedly have significant structure which can only be resolved by instruments with higher resolutions. For example, the features attributed to the helium-like ions of silicon and sulfur are expected to be composed of three separate lines whose relative intensities are a measure of the density and equilibrium state of the emitting plasma. The broad feature near 1 keV are attributed to a complex of L lines of the various ions of iron. Resolution of these lines and measurement of their relative intensities would provide a composition-independent measure of the source temperature.

These possibilities and others have motivated numerous efforts to achieve high resolution spectroscopy of cosmic X-ray sources. Much success has been achieved in the case of the Sun which is near and bright. Figure 1 presents the spectrum of a solar flare obtained by Bragg reflection spectrometry in a rocket observation by Walker and Rugge (1970). The latter shows the triplet structure of the emissions from helium-like ions of sulfur XV and silicon XIII.

To measure these interesting details of spectra, one needs resolutions of more than 100, i.e., $E/\Delta E \gtrsim 100$. Only Bragg reflection from crystals affords such resolutions in the energy range above 0.5 keV where most of the interest lies. Bragg reflection occurs for only a very narrow range of wavelengths about the value given by the Bragg formula $\lambda = (2d/n) \sin \theta$, where d is the lattice spacing, θ the grazing angle of incidence, and n an integer (generally 1). Thus Bragg reflection acts like a filter with a very narrow pass band. To observe a line one must scan this pass band back and forth over the wavelength of the line by

rocking the crystal through a small range of angles. The result is inevitably a low average throughput of line photons. Unfortunately, the brightest extrasolar sources are much fainter than a typical solar flare so that high resolution spectroscopy of extrasolar sources is much more difficult to achieve. Even with the Einstein telescope very long exposures are necessary to achieve adequate statistics.

During the 10 years since development of the FPCS began, more than 12 rocket and satellite observations of extrasolar sources with Bragg spectrometers were carried out. Two positive results were reported. One was evidence for the Lyman alpha line of Oxygen VIII in the Puppis A supernova remnant, reported by Zarnecki and Culhane (1977). The second was detection of K-alpha emission from highly ionized iron in Cygnus X-3 by the Columbia Group (Kestenbaum et al., 1978) working with their instrument on the OSO-8 satellite.

The Einstein Observatory has now provided two capabilities essential to achieving the full potentialities of high resolution spectroscopy. One is focusing optics which permits the use of an imaging spectroscope. This gains the benefits of the large collecting area of the primary mirrors while bringing the Bragg reflected X-rays to a focus on a small area of detector, thereby achieving a high ratio of signal counting rate to detector background counting rate. The other essential capability is accurate and sustained pointing which achieves long and efficient exposures. With these capabilities the FPCS attains sensitivities which are orders of magnitude greater than those achieved by previous instruments.

Table 1 summarizes the spectral resolutions required to attain various scientific objectives. Spectral features can be identified with resolutions of 10 to 30. Resolution of the helium triplets and identification of the ions responsible for lines in the L-line complex of iron requires resolutions of 100 to 300. Measurement of Doppler shifts due to bulk motions in supernova remnants need resolutions in the range 100 to 1000. The effects of thermal broadening require resolutions in excess of 1000 which are not yet attainable.

The FPCS was developed at MIT for the purpose of obtaining this new kind of astrophysical data. Herbert Schnopper and Kenneth Kalata contributed to the instrumental concept. Claude Canizares has been responsible for the scientific development of the instrument and scientific coordination of the project. Thomas Markert has been in charge of the prelaunch calibration measurements, the mission planning and the orbital operation. Garrett Jernigan supervised development of the data system. Frank Winkler has played a key role in developing the observing program, particularly the part devoted to supernova remnants. John Donaghy was in charge of the engineering effort carried out at the MIT Laboratory for Space Experiments.

Figure 2 illustrates the operation of the instrument: X-ray photons diverging from a point in the focal plane and having wavelengths near that defined by the Bragg formula for the given angle of incidence are reflected from the curved crystal to an astigmatic image in the form of a narrow line in the position sensitive proportional counter. The crystal curvature compensates for the divergence of the X-ray beam so that the angles of all rays striking the crystal are nearly the same. X-rays diverging from a different point in the focal plane, horizontally displaced from the other point, strike the crystal at a different angle, and are selectively reflected to a displaced parallel line image. Thus the instrument achieves both spectral resolution and one dimensional spatial resolution. This spatial resolution is useful in the study of extended sources such as supernova remnants.

For the spectrometer to function as described, the entrance aperture, curved crystal and detector must lie on the circumference of the "Rowland Circle." This condition is achieved for any desired angle of incidence on the crystal with gears and slides driven by stepping motors controlled through telemetry according to procedures incorporated in the mission operation program. The instrument is mechanically complex; however, it has functioned flawlessly since launch. An assembly drawing is shown in Figure 3, and a list of its properties is given in Table 2.

Figure 4 shows the profile of the line image at the spectrometer detector of a distant point source of 1.5 keV aluminum K-alpha radiation obtained during calibration tests here at MSFC. Selecting only those events detected in the image, we plot their frequency as a function of the angle of incidence on the crystal. The result is the "rocking curve" shown in Figure 5. It shows the response of the instrument to a narrow spectral line.

I turn now to the results obtained so far on three very different kinds of X-ray sources: a compact X-ray star, a diffuse supernova remnant, and an extended halo around an external galaxy. The compact X-ray star is Sco X-1, the brightest persistent X-ray source in the sky, and therefore a favorite target of previous efforts at Bragg Spectrometry. Those efforts have shown no evidence of line emission and have placed upper limits on such emissions which are far below the line strengths expected for an optically thin plasma with solar composition at the temperature of Sco X-1. This has led to the conclusion that Sco X-1 is an optically thick source in which multiple electron scatterings alter the wavelengths of escaping photons and thereby broaden emission lines to the point of undetectability. Sco X-1 was an early target of FPCS observations carried out by Christophe Berg. Figure 6 is the Bragg reflected image of Sco X-1 near the wavelength of the iron L-lines. Figure 7 is the pulse height distribution of the X-ray photons recorded in the image. There are two peaks corresponding to the energies of the first (n = 1) and second (n = 2) order Bragg reflected photons. Figure 8

is the rocking curve in the wavelength range of the iron L lines. No lines are seen and from this we have further reduced the upper limits on the line emission from Sco X-1 (Table 3).[1]

We have examined several supernova remnants including Cas A which has been shown by the Solid State Spectrometer to have strong lines of the helium-like ions of silicon and sulfur. Figure 9 shows the FPCS rocking curve of the sulfur XV line which has been analyzed by Frank Winkler. It is clearly broader than the aluminum K-alpha line observed during the calibration tests. The various possible contributions to the line width are indicated in the figure. The effects of spatial extent obscure the intrinsic structure of the line so that we have not yet determined the relative strengths of the triplet components.

Last week we received the first data from the observation of the Puppis A supernova remnant. Figure 10 is the rocking curve for the Lyman alpha line of Oxygen VIII. The curve on the bottom is the exposure as a function of the Bragg angle. This is a crucial part of every analysis. Data are accumulated from many observations during which the crystal is rocked slowly back and forth. We therefore must keep an accurate account of the exposure we have at each Bragg angle to make sense out of the observed numbers of events. The rocking curve shows a very strong emission line. Only about one-sixth of the supernova remnant image was included in the aperture of the spectroscope. If one multiplies the apparent line emissivity by the ratio of the total area of the remnant to the area that was examined, one finds a line intensity which is consistent with that found previously by Zarnecki and Culhane.

Finally, I turn to the study of M-87 which is a giant elliptical galaxy with an X-ray emitting halo whose overall spectrum has been characterized as that of an optically thin plasma with a characteristic temperature of 2.6 keV. The K line of iron has been detected previously in the X-ray spectrum. This was clear evidence for the presence of heavy elements in the region around M-87 and led to the conclusion that the emitting gas is not primordial, but rather that it was stripped out of other galaxies in the Virgo cluster and is now falling into the potential well of M-87. As it falls, its kinetic energy is converted into heat, and as the density rises the rate of cooling by radiation increases. Model calculations have been made to predict the temperature profile across the halo region. The observed intensities of various emission lines can be used, in principle, to test the validity of such a temperature profile. The Lyman alpha line of oxygen VIII should be particularly useful in such a test because it is strong at temperatures lower than 2.6 keV. Figure 11 shows the discovery of this line in the rocking curve obtained

---

1. Since this report was given a broad OVIII line has been detected.

by Claude Canizares. The observed line flux implies a luminosity at the source of 1.2×10^{42} ergs s^{-1}. A search was also made for the L lines of ionized iron, but only upper limits have been obtained so far. The measured intensity of the oxygen VIII line is more than seven times greater than expected for an isothermal gas with the cosmic abundance ratio of oxygen to iron at 2.6 keV. The results show that substantial amounts of cooler gas at temperatures of 10^7 K or less are present in the vicinity of M-87.

Only a fraction of the production data from the long FPCS exposures has been received so far. Thus we have only begun our exploration of what promises to be a highly productive new area of research in X-ray astronomy.

Note: As of July 11, 1979 a total of nine emission lines had been detected in the spectra of galactic and extragalactic objects by the FPCS and there were strong indications of the presence of an additional seven lines.

BIBLIOGRAPHY

Kestenbaum, H. L.; Ku, W. H. M.; Long, K. S.; Silver, E. H.; and Novick, R., 1978, Ap. J., 226, 282.

Walker, A. B. C. and Rugge, H. R., 1970, Astron, Astrophys., 5, 4.

Zarnecki, J. C. and Culhane, J. L., 1977, Mon. Not. R. Astr. Soc., 178, 57P.

TABLE 1. COSMIC X-RAY SPECTROMETRY

Purpose	Required Resolutions ($E/\Delta E$)
Element Identification	10 - 30
Iron Ion Abundances (temperature)	>100
Helium Triplet Intensities (densities and equilibria)	>100
Doppler Shifts in SNR	100 - 1000
Thermal Broadening	>3000

TABLE 2. EINSTEIN OBSERVATORY FOCAL PLANE CRYSTAL SPECTROMETER

Range	0.2 - 3.0 keV
Resolving Power ($E/\Delta E$)	50 - 500
"Effective Area"	~0.5 cm^2 (single line)
Required Observing Times	10^4 - 10^5 sec

TABLE 3. SCO X-1

Line	3σ Upper Limit Equivalent Width (eV)	Model
Fe 23/24	1.0	Thermal
Fe 17 (11Å)	2.5	Thermal
Fe 17 (15Å)	1.7	Thermal
OVIII Recombination	1.0	Nebular Fluorescence
OVIII Ly α	1.3	Nebular Fluorescence
Fe 1	1.3	Stellar Fluorescence

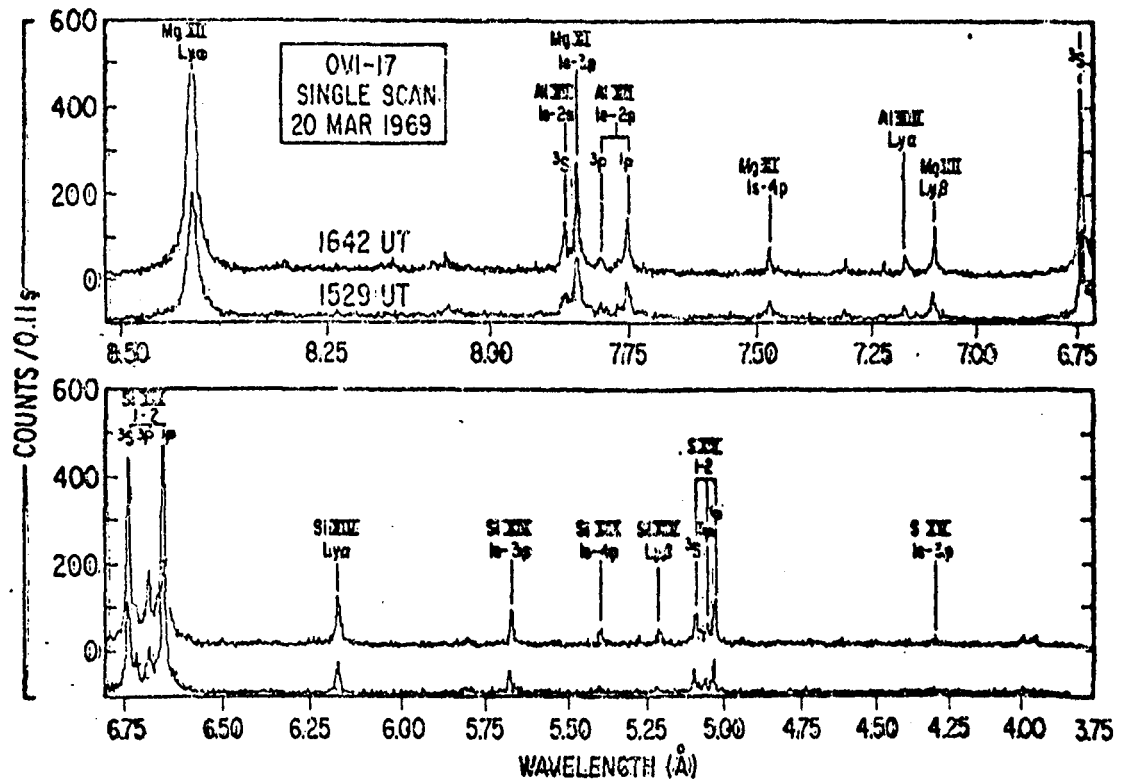

Figure 1. Solar X-ray spectrum between 4 and 8.5 Å during a period of high solar activity obtained by a rocket-borne Bragg reflection spectrometer by Walker and Rugge (1970).

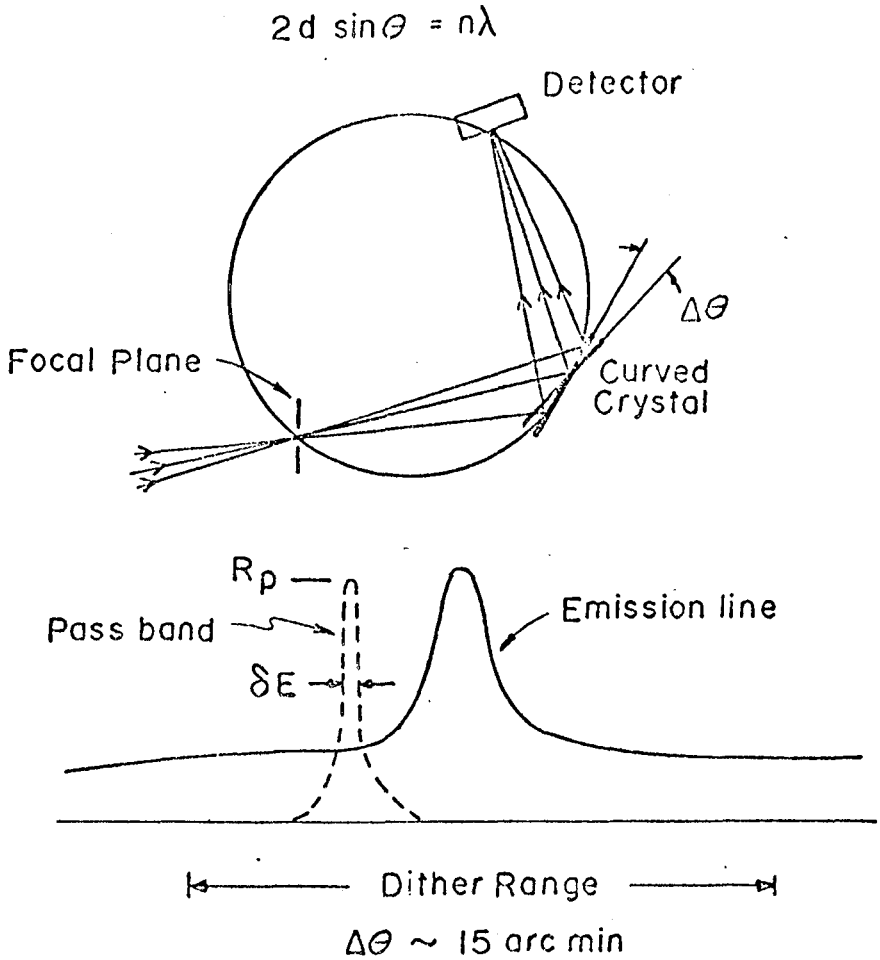

Figure 2. Schematic diagram of Bragg spectrometer.

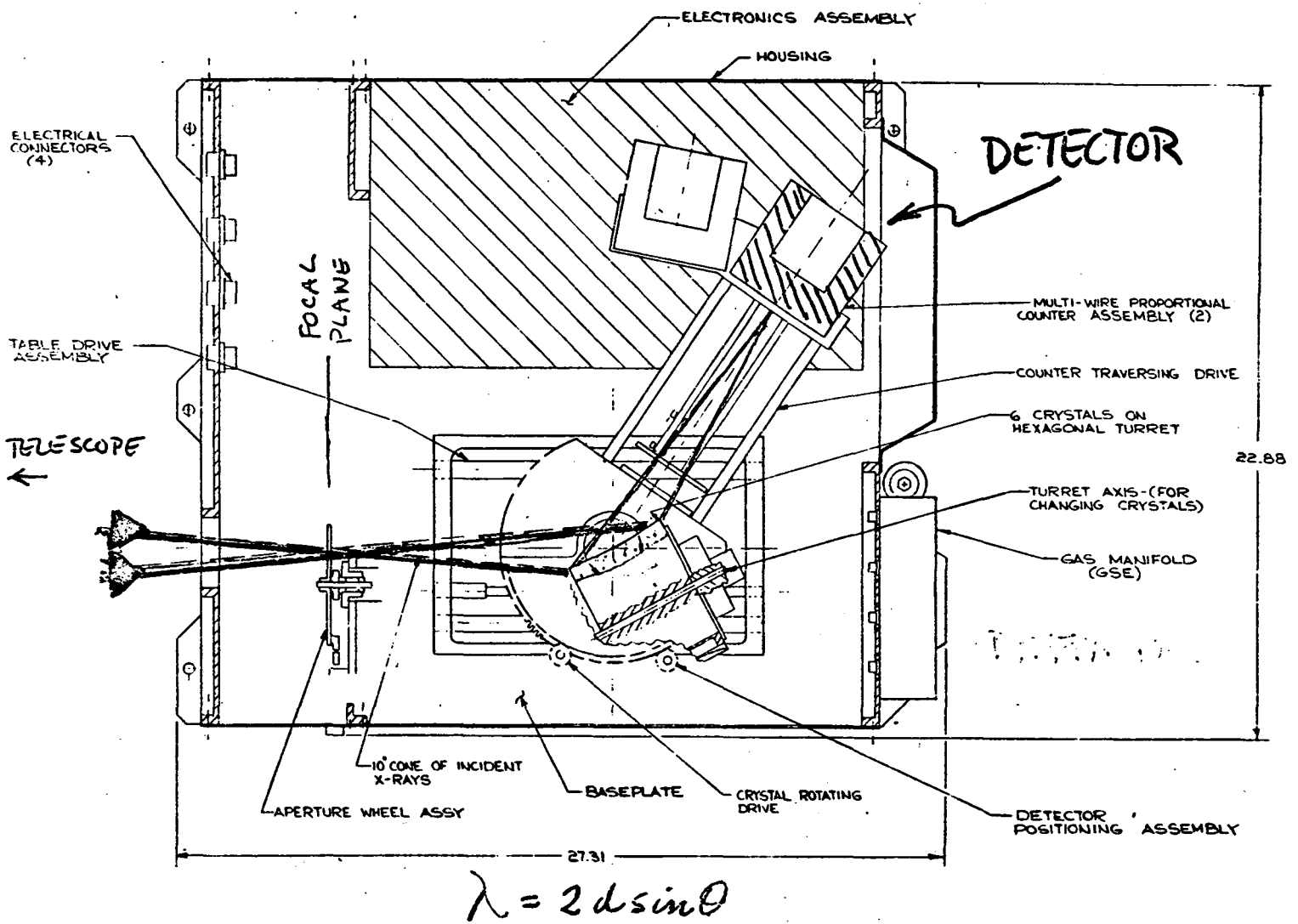

Figure 3. Assembly drawing of the MIT Focal Plane Crystal Spectrometer.

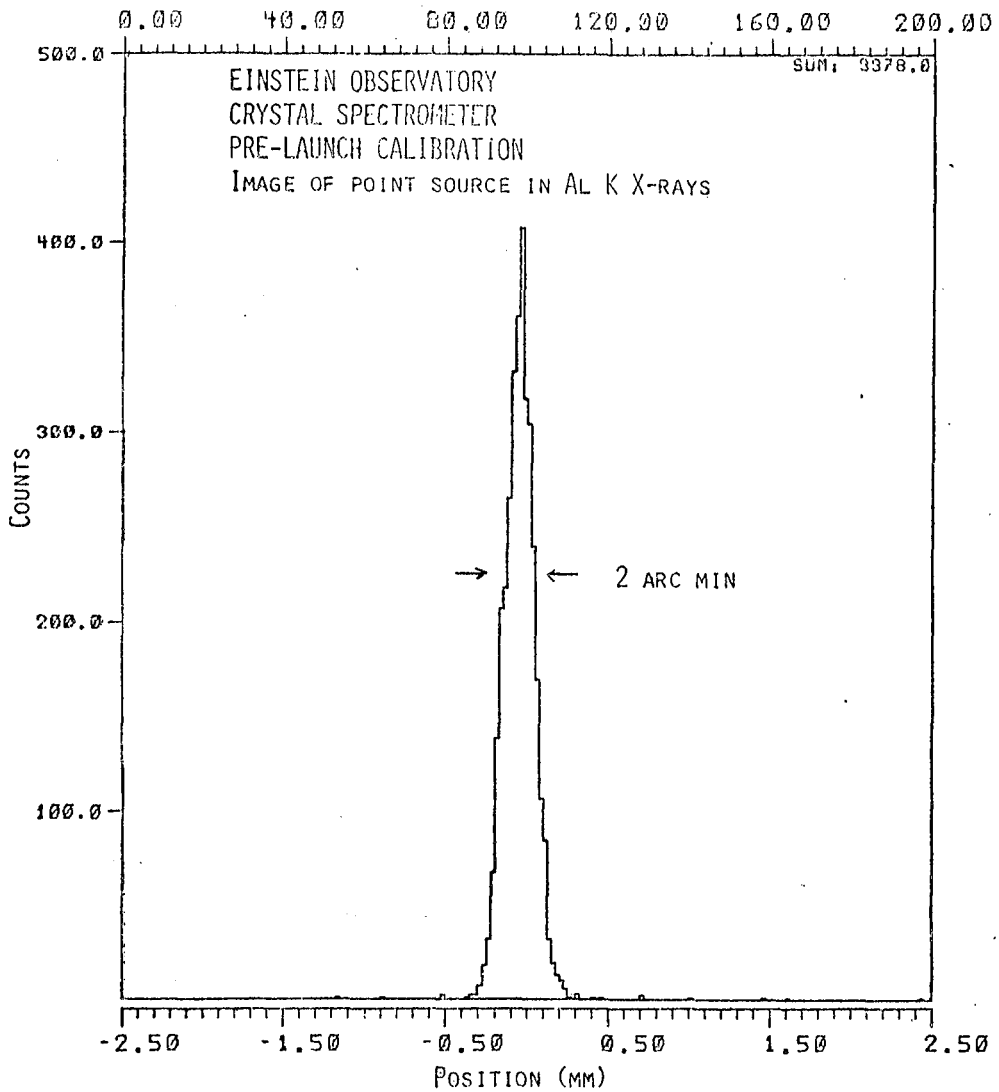

Figure 4. Bragg-reflected image of a point source of Al K X-rays obtained during prelaunch calibration tests.

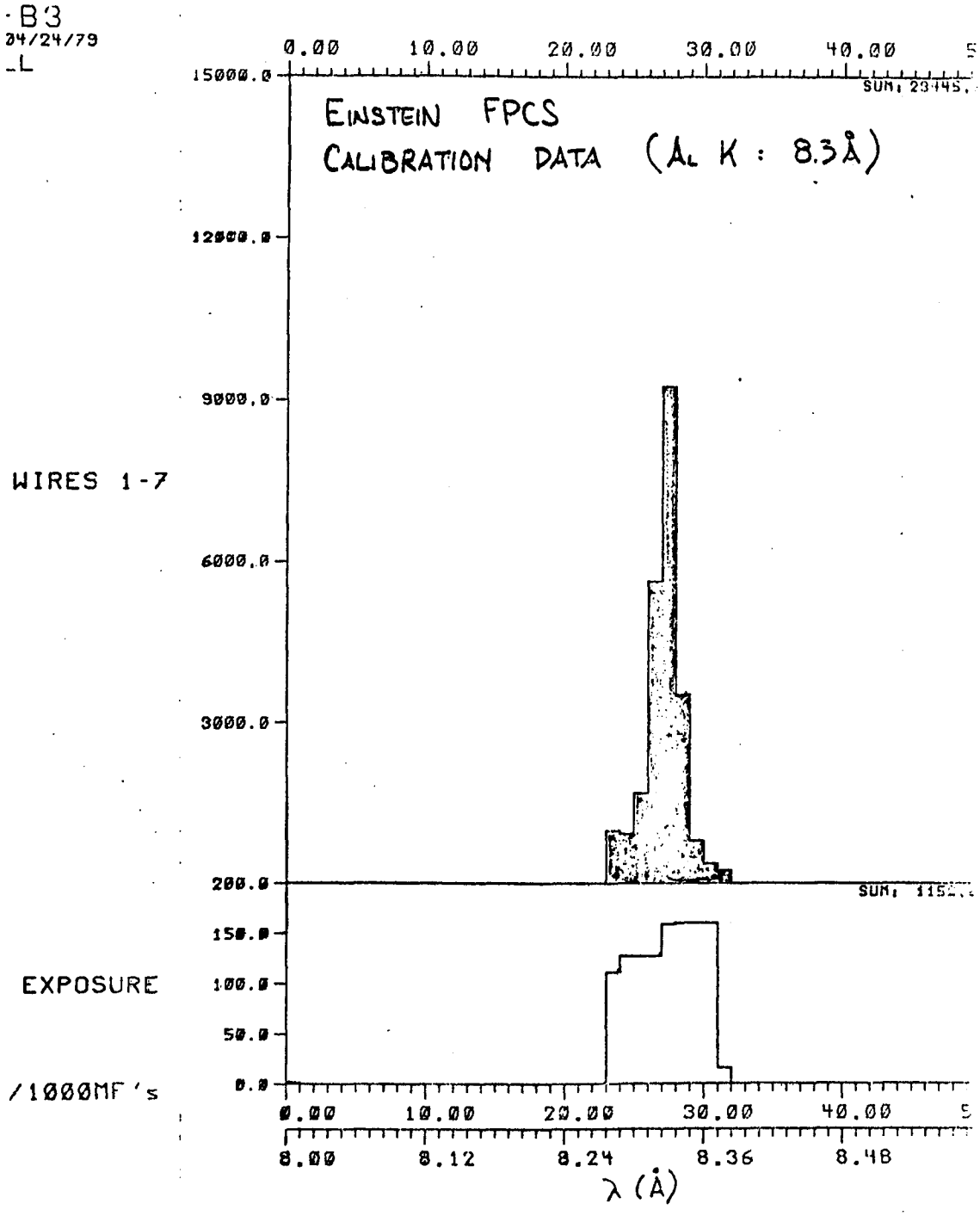

Figure 5. Rocking curve of Al K X-rays obtained during prelaunch calibration tests.

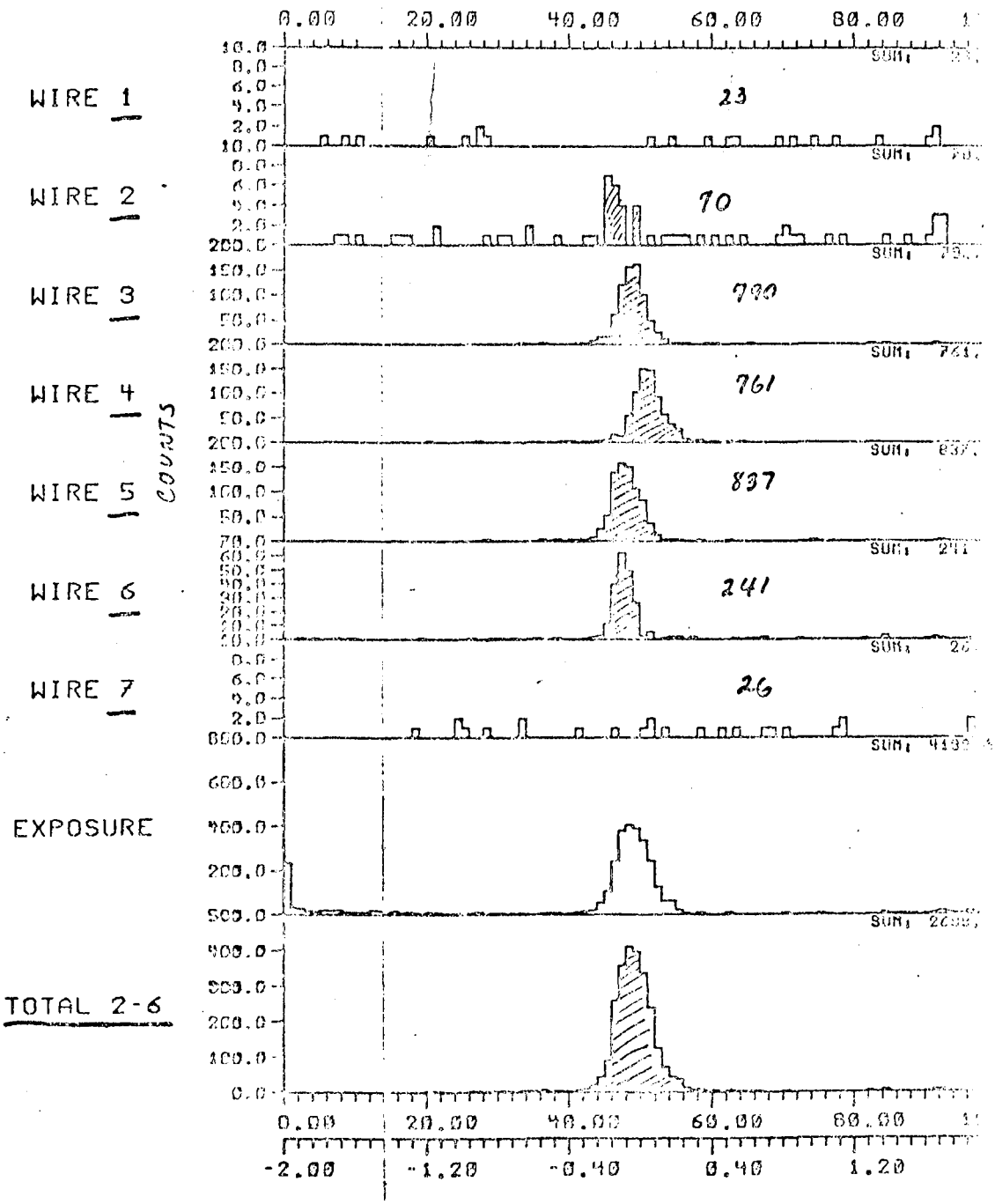

Figure 6. Bragg-reflected image of Sco X-1 near 1 keV.

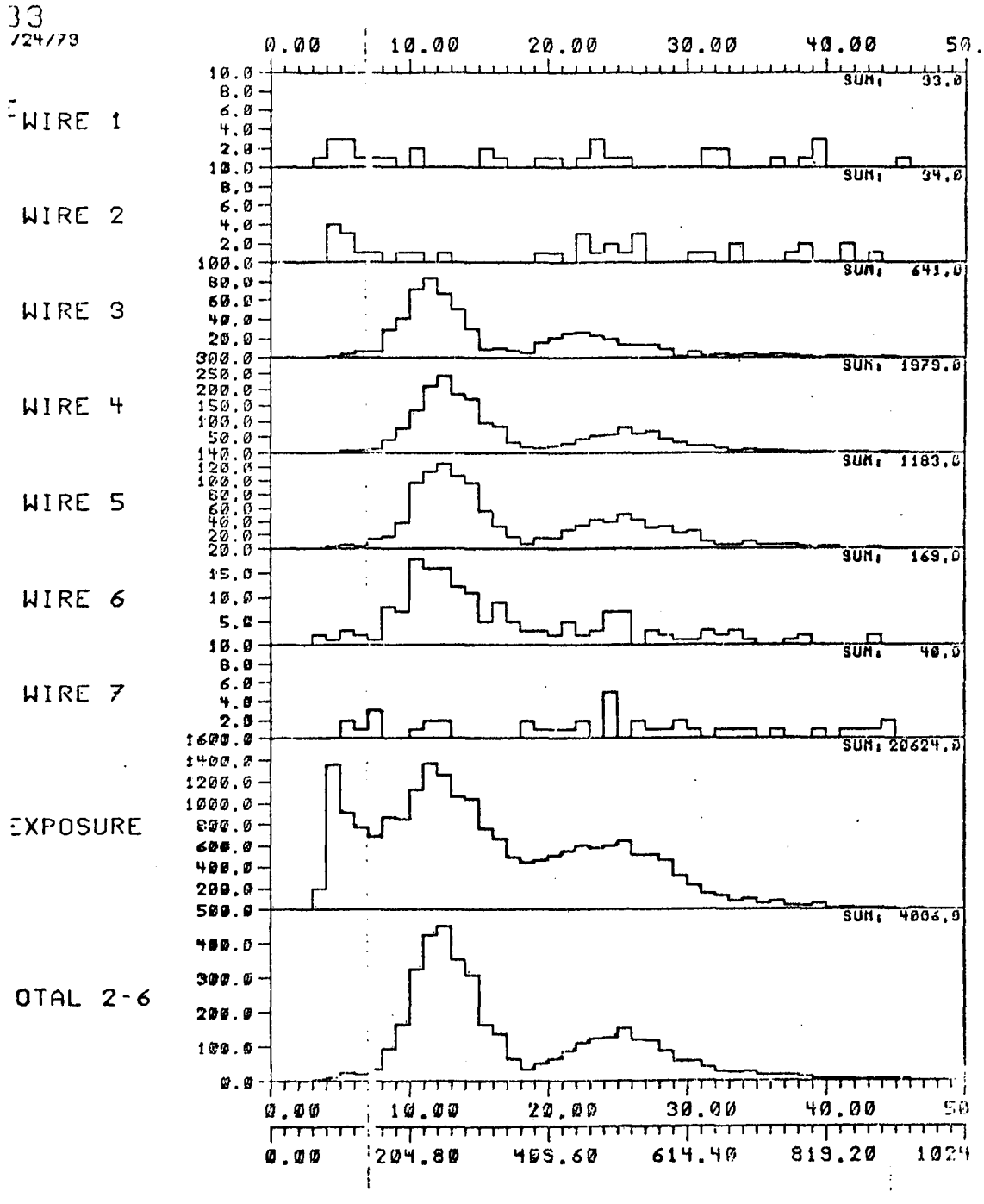

Figure 7. Pulse height distribution of Bragg-reflected X-rays.

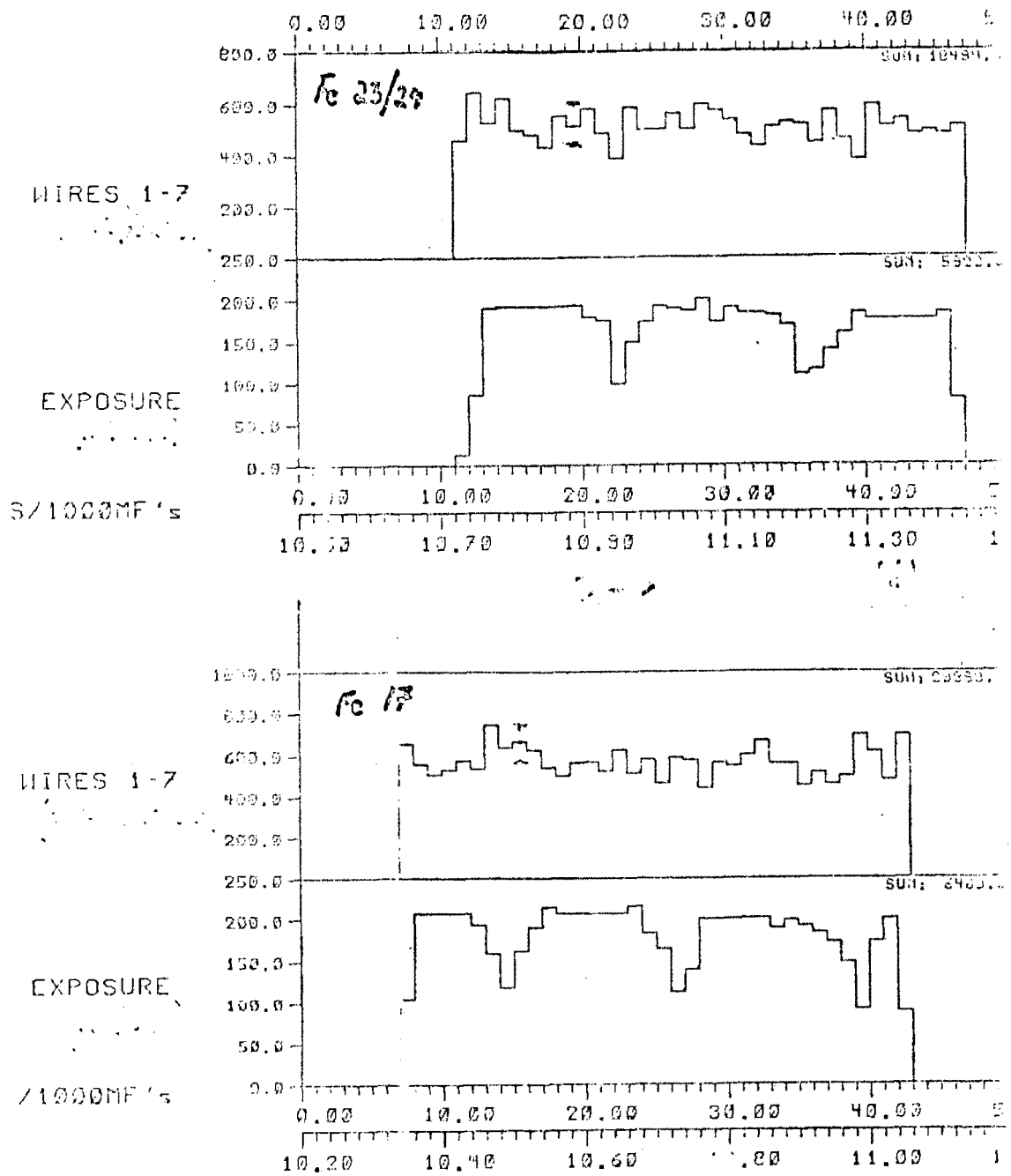

Figure 8. Rocking curve of Sco X-1 spectrum of wavelengths of iron L lines.

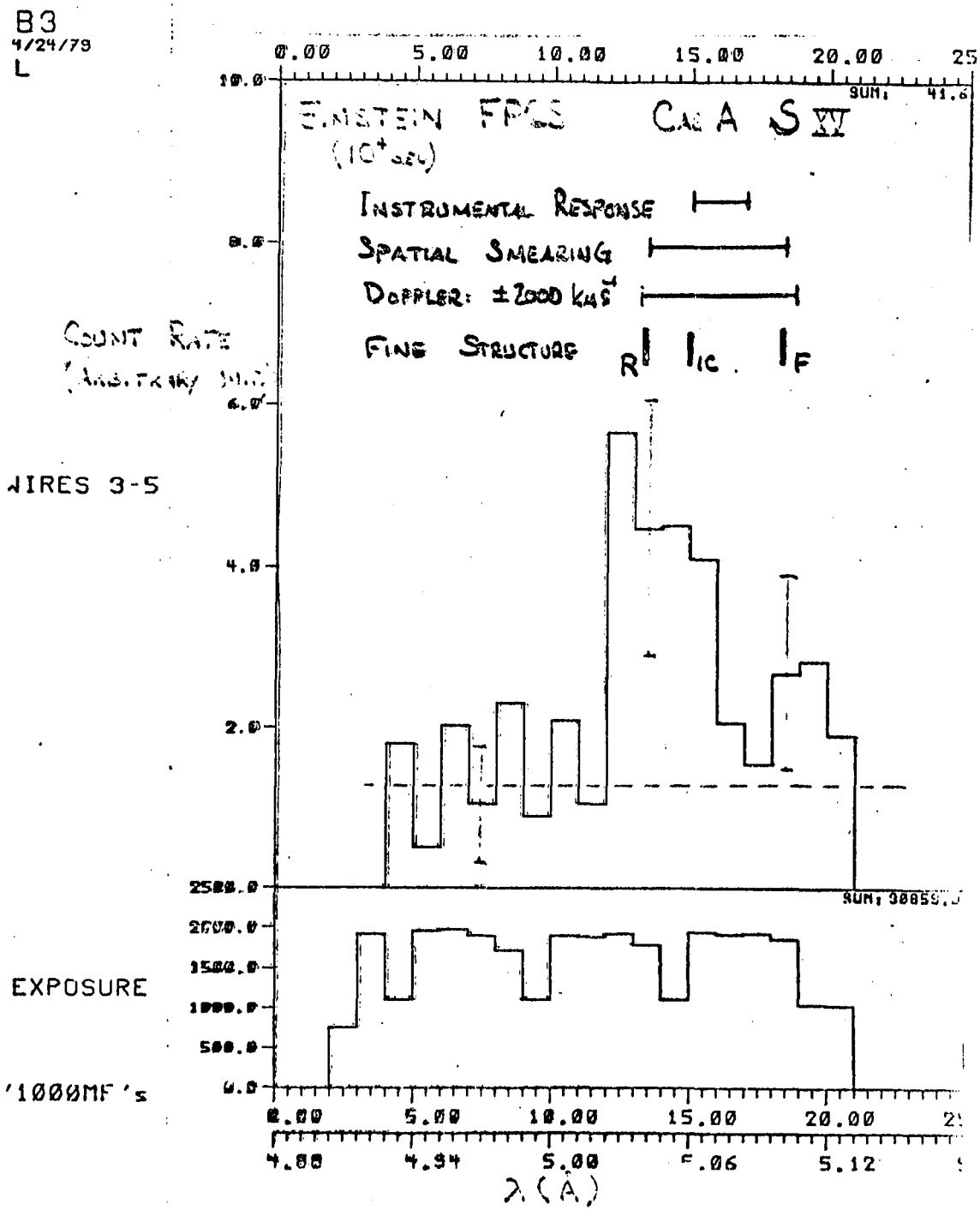

Figure 9. Rocking curve of sulfur XV line in Cas A.

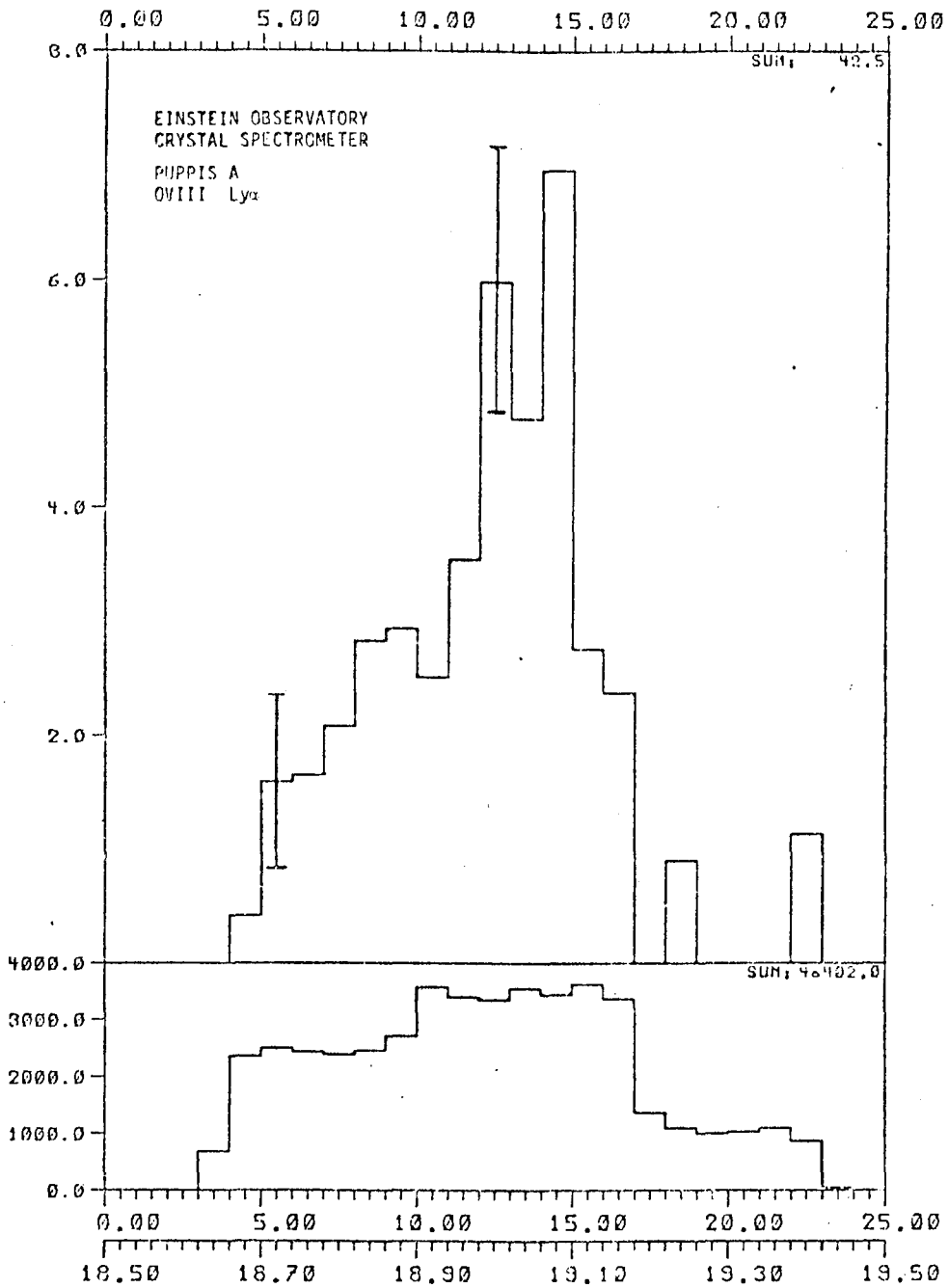

Figure 10. Rocking curve of oxygen VIII Lyman alpha line on Puppis A.

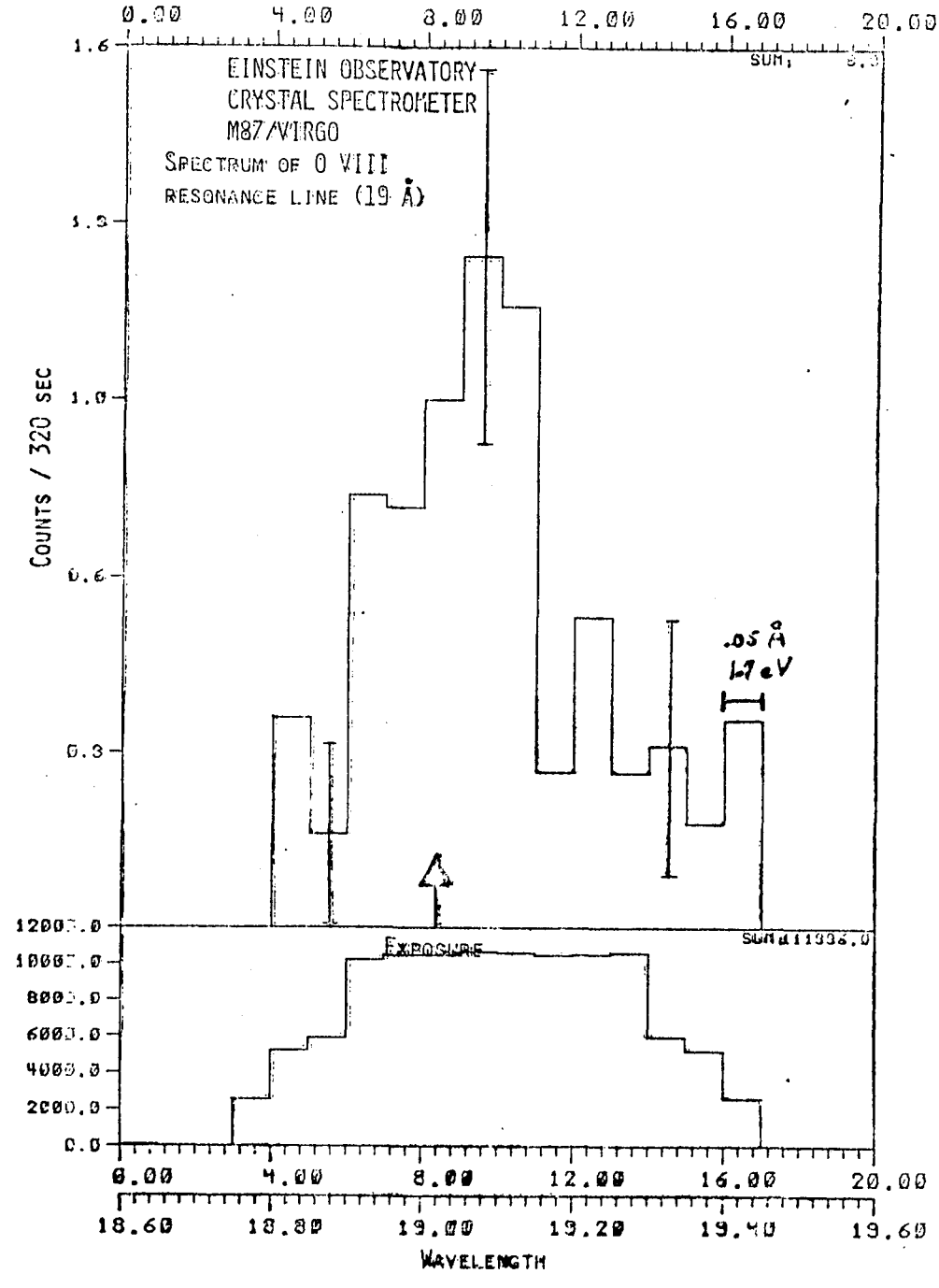

Figure 11. Rocking curve of oxygen VIII Lyman alpha line in M-87.